LCLS-II Technical Note

OPTIMIZATION OF COMPENSATION CHICANES IN THE LCLS-II BEAM DELIVERY SYSTEM

LCLS-II TN-15-41

11/23/2015

J. Qiang, M. Venturini

1 Introduction

The microbunching instability seeded by shot noise and driven by collective effects (primarily space-charge) can significantly degrade beam quality before the electron bunches are delivered to the FEL undulators. Figure 1 shows a schematic layout of the LCLS-II beam delivery system [1, 2].

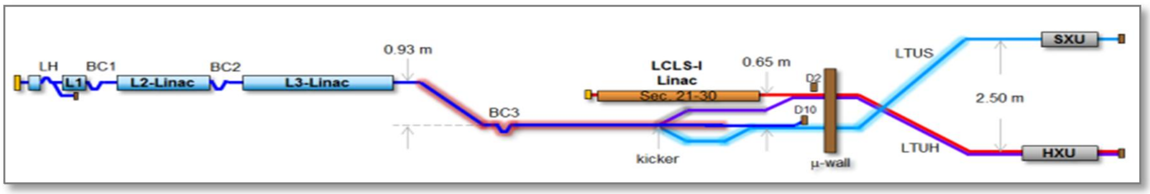

Figure 1: Schematic layout of LCLS-II.

In our earlier studies, we identified beam transport trough the long beamline from the exit of the Linac to the entrance of the FELs as particularly problematic from the standpoint of the instability. This is illustrated by the left pictures of Fig. 2A showing beam phase-space and current profile as observed at the entrance of the HXR FEL undulator and simulated with IMPACT (see Sec. 2). The simulation was made by tracking a macroparticle model of a 100 pC bunch, starting from the exit of the second bunch compressor (BC2). The bunch-distribution model is a short flat-top with I = 900A peak current and Gaussian slice energy density with about 0.5 MeV rms spread. The distribution is created using a random number generator to populate the phase space, thus resulting into the same level of shot noise expected in a physical bunch, as in our simulations the macroparticle charge is the same as that of the physical electrons. A large instability is observed in the sub$-\mu$m range, resulting from the combination of a long (> 2 km) transport line, the presence of several doglegs and other dispersive transport sections, and a relatively low (compared to LCLS) beam energy (4 GeV).

To mitigate the effect we proposed [3] to modify the lattice so as to introduce local compensation of the momentum compaction function (R_{56}), thus preventing the longitudinal slippage responsible for the appearance of microbunching. A simple way to realize local compensation is to place weak 4-dipole chicanes (contributing negative R_{56}) next to the main dipoles of the transport line (contributing positive R_{56}). The benefit of these compensation chicanes is demonstrated by the right pictures of Fig. 2A, showing a much flatter current profile.

Use of compensation chicanes has been adopted in the present July-2015 lattice baseline data set. Specifically, two compensation chicanes are placed at the two ends of DL1, the dogleg that takes the beam into the bypass line. The main dispersive sections in the HXR transport line downstream of the spreader consist of two double-bend achromats arranged into a dogleg configuration. Because of space constraints, compensation chicanes are placed next to each of the two dipoles of the first double-bend achromat but only one chicane is used in the second double-bend achromat. In the latter case compensation is not highly localized but was found to be adequate. Similarly, two compensation chicanes are inserted in the SXR transport line.

While more complete macroparticle simulations including tracking starting from the injector (vs. starting from BC2 as in Fig. 2A) confirmed the effectiveness of the compensating chicanes they also indicated that they were not sufficient to eliminate microbunching completely for the nominal setting of laser heating [4]. This is particularly evident in the beam transported to the SXR FEL, see Fig. 2B. We found that some of the microbunching was due to an interesting 3D effect [5] occurring in the doglegs of the transport line downstream of the Linac. Transverse space-charge fields in these dispersive regions can induce significant longitudinal slippage and hence contribute to microbunching because of a finite R_{52} if some energy modulation along the beam is present (e.g. due to microbunching instability developed upstream). Luckily, the direction of the transverse space-charge induced slippage can be countered by R_{56}-induced slippage, opening up the possibility that retuning the compensating chicanes may yield better overall control over the instability compared to exact R_{56} compensation -- this possibility was recognized in [5]. While we do not have an analytical demonstration yet, the numerical simulations presented here show that indeed there exists an optimal setting for the compensation chicanes for suppression for the instability.

The results of these simulations are discussed in Sec. 3, after a brief description of the computational tools in Sec. 2. In Appendix A we report results from additional numerical work made to highlight the role of transverse space charge.

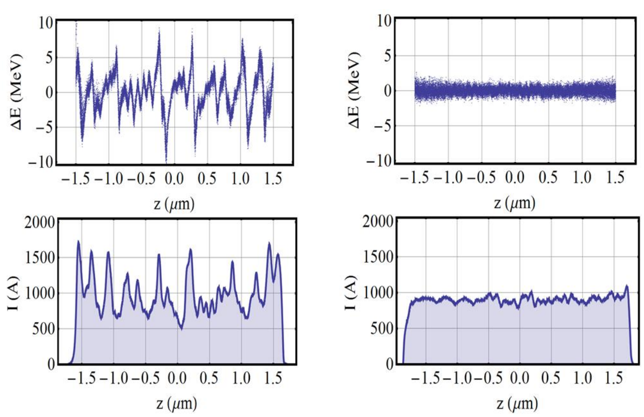

Figure 2A. Section of the bunch observed at the entrance of the HXR FEL for the March 2014 Baseline Lattice (left) and for the lattice modified with the insertion of compensation chicanes (right) showing much reduced instability. The top (bottom) pictures show the longitudinal phase space (current profile). The beam tracked here is an idealized model of a 100 pC bunch with flat-top in current profile and Gaussian slice energy distribution. Tracking started from the exit of BC2 and therefore microbunching effects upstream of BC2 are not captured.

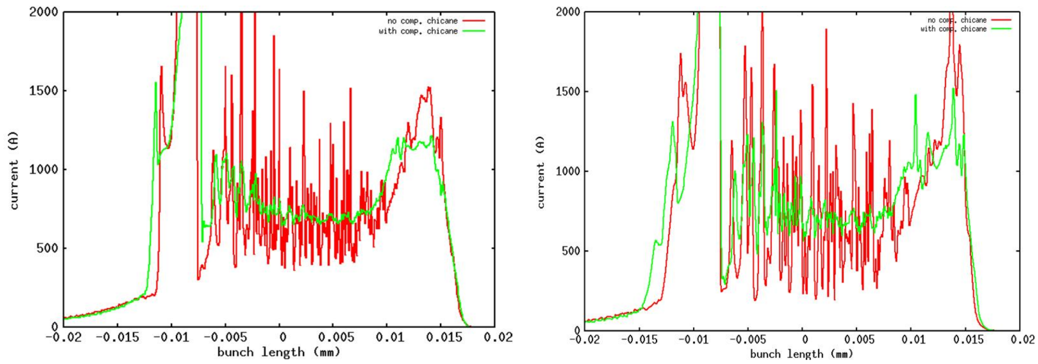

Fig. 2B: Current profiles at the entrance of the HXR (left) and SXR FEL (right) undulators contrasting the lattice with (green) and without (red) compensation chicanes. (Start-to-end simulations of a 100 pC bunch.)

2 Computational setup

All simulations presented in this study were done using a 3D parallel beam dynamics simulation framework IMPACT [6-8]. It includes a time-dependent 3D space-charge code module IMPACT-T to simulate photo-electron beam generation and acceleration through the photo RF gun, buncher and boosting cavities, and a position-dependent 3D space-charge code module to simulate electron beam transport through the superconducting linac system. Besides the 3D space-charge effects, the simulation also includes coherent synchrotron radiation (CSR) effects through a bending magnet, incoherent synchrotron radiation inside the bending magnet, RF cavity structure wakefield, and resistive wall wakefield. All simulations were done using the real number of electrons for three bunch charges, 20 pC, 100pC, and 300pC, to capture the initial shot noise of the beam, which can have important impact on the final beam quality and FEL performance due to the microbunching instability.

3 Optimization results

In this optimization, we scanned the bending angle of all bending magnets in all compensation chicanes by a same percentage factor. The 0 percentage corresponds to the nominal design settings. The core of the final current profile at the entrance of the undulator was fitted by a cubic polynomial. The rms current fluctuation was calculated using the difference between the final core current and the fitted current profile. Figure 3 shows the rms current fluctuation as a function of the percentage of over compensation for the 100 pC hard x-ray scenario. It is seen that 20% increase in the beam angle (corresponding to about a factor 1.5 over compensation of R_{56}) yields the least current fluctuation. Figure 4 shows the final longitudinal phase space and current profile with the nominal compensation setting and the 20% over compensation setting. The 20% over compensation setting yields much less microbunching fluctuation in both the phase space and the current profile. Figure 5 shows the rms current fluctuation as a function of the percentage of over compensation for the 100 pC soft x-ray scenario. The 20% over compensation setting yields minimum rms fluctuation even though 15% over compensation has almost the same rms fluctuation. Figure 6 shows the final longitudinal phase space and current profile without and with 20% over compensation. Again, the 20% over compensation setting results in much less energy and current modulation.

We also optimized the compensation chicanes for the 300 pC scenario. Figure 7 shows the final rms current fluctuation as a function of the over compensation percentage of the chicane through the hard x-ray beam line. It is seen that 15% over compensation yields the least current fluctuation. Figure 8 shows the final phase space fluctuation and current profile without and with 15% over compensation. It is seen that the 15% over compensation chicane setting results in less modulation than the nominal setting. Figure 9 shows the final rms current fluctuation as a function of the over compensation percentage through the soft x-ray beam line. The 10% over compensation setting has the least fluctuation while the 15% over compensation yields about the same fluctuation level. Figure 10 shows the final longitudinal phase space and current profiles without and with 15% over compensation. Again, 15% over compensation shows less phase space and current fluctuation compared with the nominal compensation chicane setting.

In the third scenario with 20 pC charge, we did the same optimization of the bending angle of the bending magnets in those compensation chicanes. Figure 11 shows the rms final current fluctuation as a function of over compensation percentage through the hard x-ray beam line. It is seen that the fluctuation approaches the minimum with 30% over compensation. Figure 12 shows the final longitudinal phase space and current profile with and without 30% over compensation through the hard x-ray beam line. The over compensated chicane setting shows less current fluctuation. Figure 13 shows the rms final current fluctuation as a function over compensation percentage through the soft x-ray beam line. The 20% over compensation yields the least current fluctuation. Figure 14 shows the final longitudinal phase space and current profile with and without 30% over compensation. The over compensated chicane setting has less current fluctuation than the nominal design.

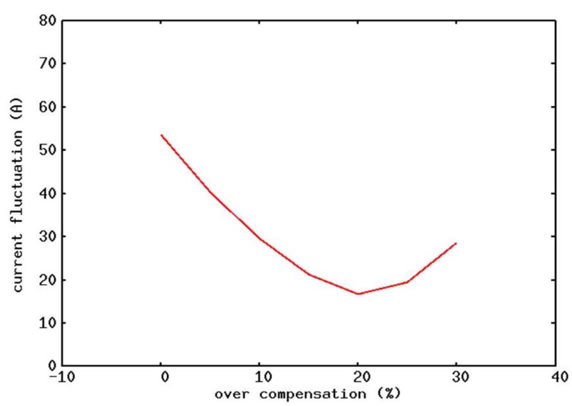

Fig. 3: RMS current fluctuation as a function of over compensation percentage of the compensation chicane setting in the 100 pC hard x-ray scenario.

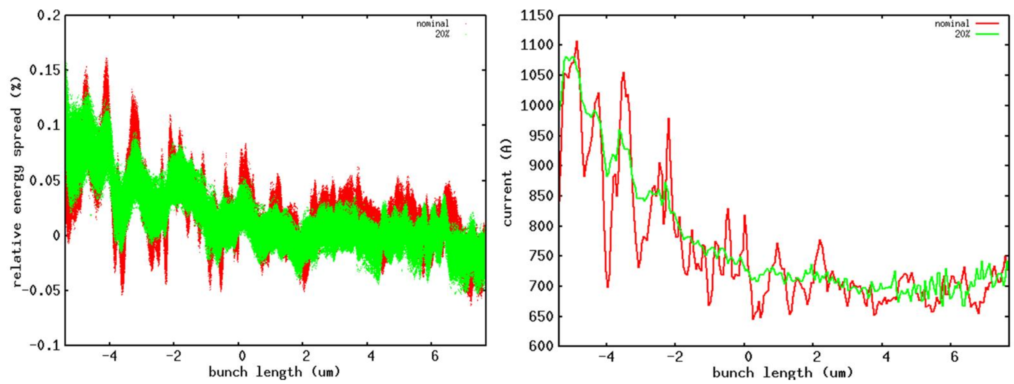

Fig. 4: Final longitudinal phase space (left) and current profile (right) with nominal and 20% over compensation settings in the 100 pC hard x-ray scenario.

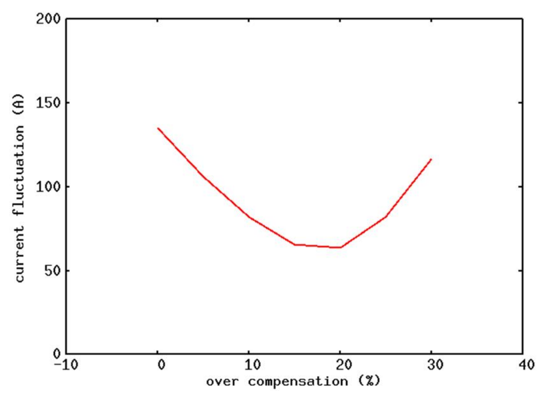

Fig. 5: RMS current fluctuation as a function of over compensation percentage of the compensation chicane setting in the 100 pC soft x-ray scenario.

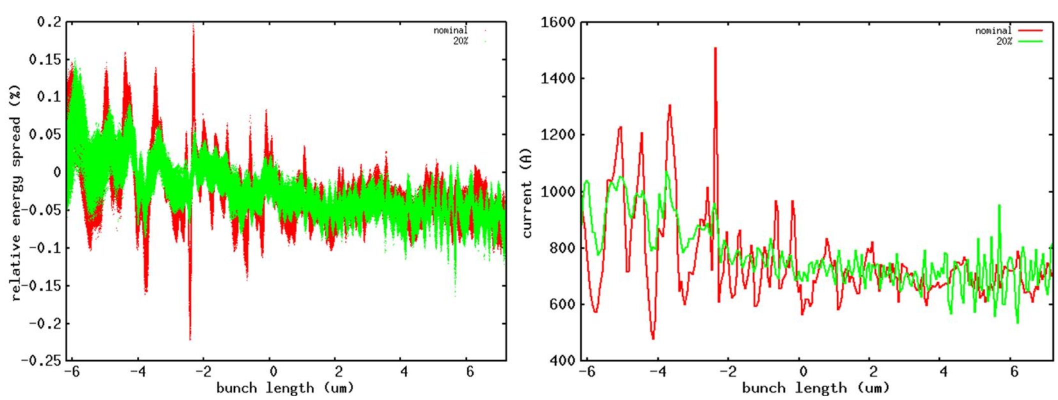

Fig. 6: Final longitudinal phase space (left) and current profile (right) with nominal and 20% over compensation settings in the 100 pC soft x-ray scenario.

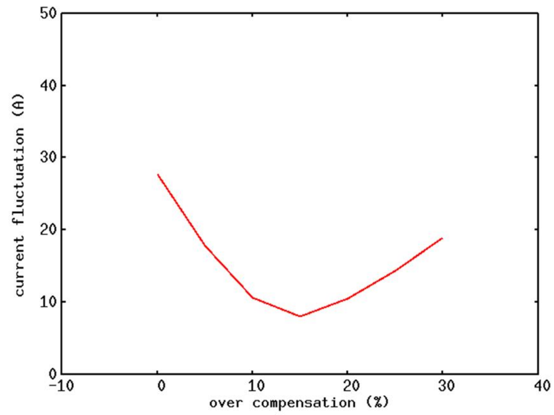

Fig. 7: RMS current fluctuation as a function of over compensation percentage of the compensation chicane setting in the 300 pC hard x-ray scenario.

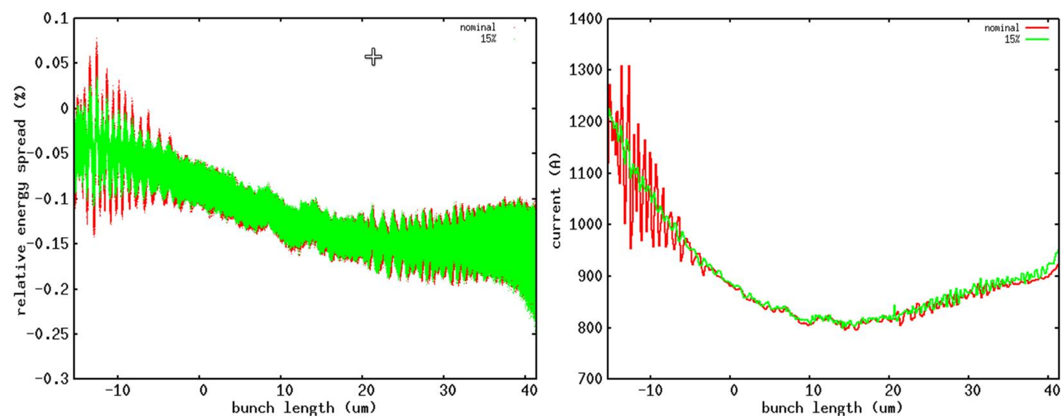

Fig. 8: Final longitudinal phase space (left) and current profile (right) with nominal and 15% over compensation settings in the 300 pC hard x-ray scenario.

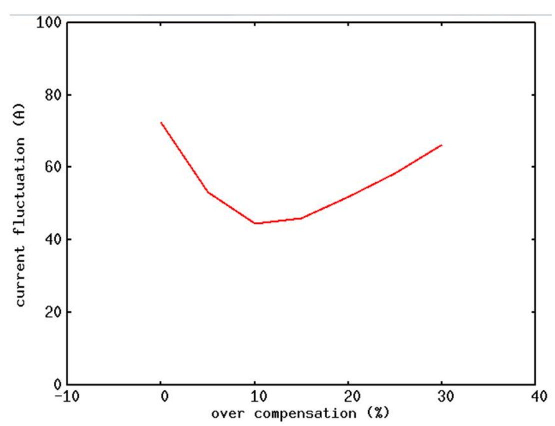

Fig. 9: RMS current fluctuation as a function of over compensation percentage of the compensation chicane setting in the 300 pC soft x-ray scenario.

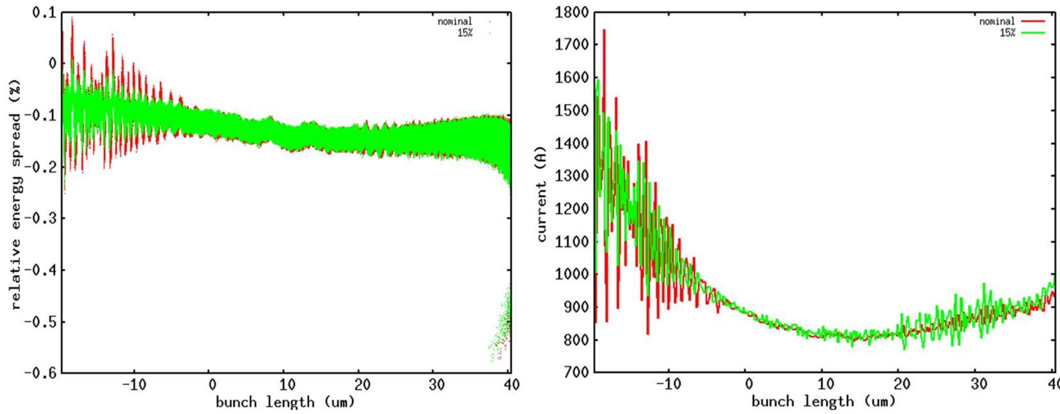

Fig. 10: Final longitudinal phase space (left) and current profile (right) with nominal and 15% over compensation settings in the 300 pC soft x-ray scenario.

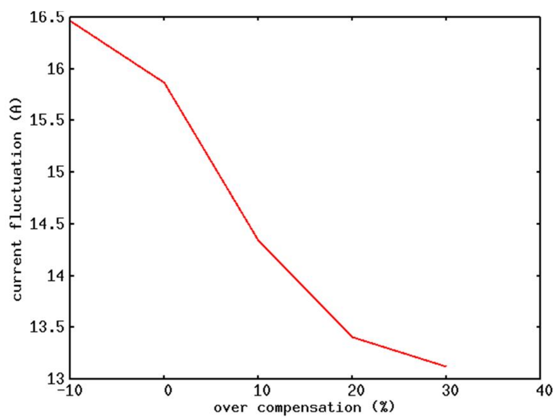

Fig. 11: RMS current fluctuation as a function of over compensation percentage of the compensation chicane setting in the 20 pC hard x-ray scenario.

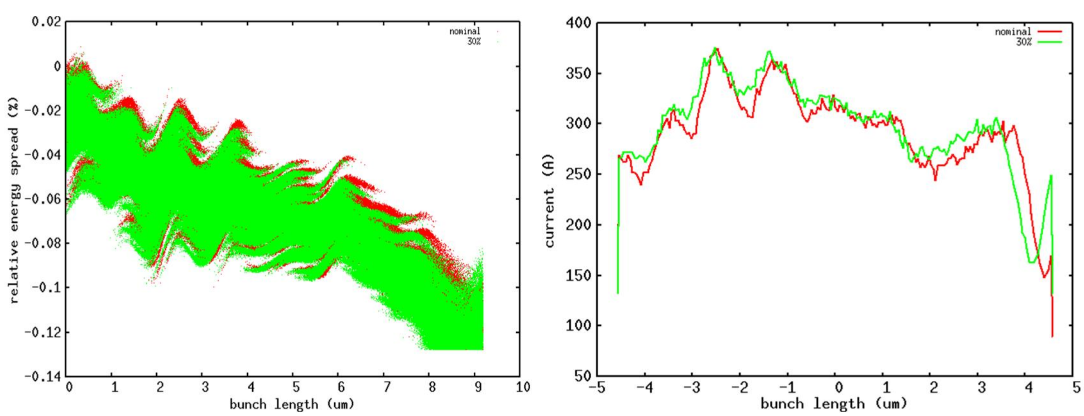

Fig. 12: Final longitudinal phase space (left) and current profile (right) with nominal and 30% over compensation settings in the 20 pC hard x-ray scenario.

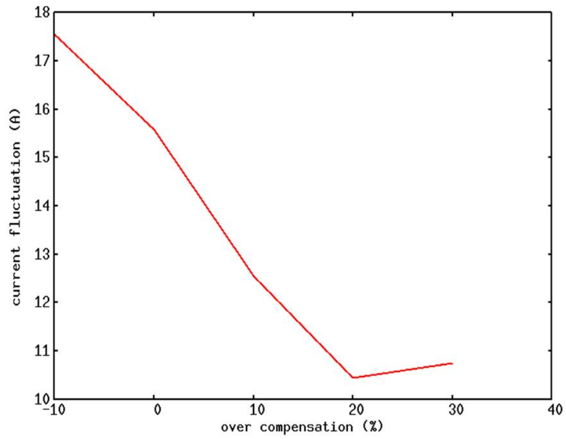

Fig. 13: RMS current fluctuation as a function of over compensation percentage of the compensation chicane setting in the 20 pC soft x-ray scenario.

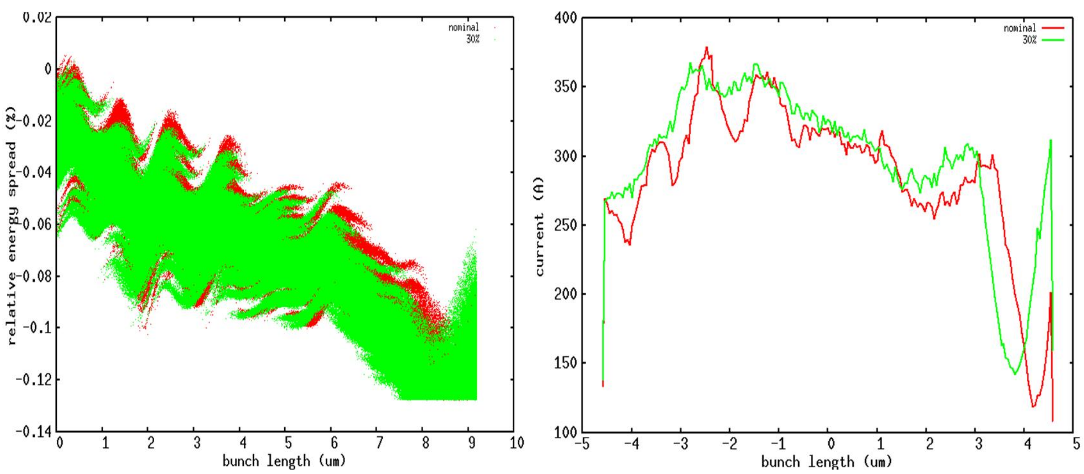

Fig. 14: Final longitudinal phase space (left) and current profile (right) with nominal and 30% over compensation settings in the 20 pC soft x-ray scenario.

4 Summary

In summary, for the 100 pC scenario, 15 – 25 percentage larger bending angle in those compensation chicanes helps reduce the microbunching induce final current and energy fluctuation significantly. For the 300 pC case, 10 – 20 percentage over compensation helps reduce the final modulation. For the 20 pC case, 15 to 30 percentage improves the beam current profiles. An interesting question deserving additional study is whether the number of compensation chicanes could be reduced without affecting their effectiveness. These new optimized compensation chicanes will be included in the Feb-2016 data set.

Appendix A

The appearance of microbunching requires two features: the generation of an uneven energy profile along the bunch (caused by collective effects) and slippage in the particle longitudinal coordinate. In an ultrarelativistic beam the latter is suppressed if the transfer matrix entry $R_{56}(s \rightarrow s_f) \simeq 0$ for any position s where *longitudinal* collective forces are non-negligible. This is the mode of operation when the compensation chicanes are tuned for local cancellation of R_{56} generated by the dipoles in the transport line and is illustrated by the red data points of Fig. 15. Minimum microbunching occurs for $r = 1$ (see caption in the figure for the meaning of r).

Longitudinal slippage can occur also as a result of changes of the angular particle coordinate (*e.g.* x') due to the *transverse* component of collective forces, if these are non-negligible at locations along the transport line where R_{52} is finite (*e.g.* within a dogleg).

The combination of transverse space-charge and longitudinal space-charge induced slippages is to modify the compensating chicanes setting where the observed bunching is minimum, blue data points in Fig. 15.

The simulations carried out for Fig. 15 where obtained by tracking an idealized macroparticle bunch model in the form of a water-bag distribution starting from the exit of the injector and having the same characteristics (emittance, current profile) as a nominal 100 pC beam. The optimum setting $r = 1.5$ is very close to that found in the Sec. 3 for start-to-end simulation beams.

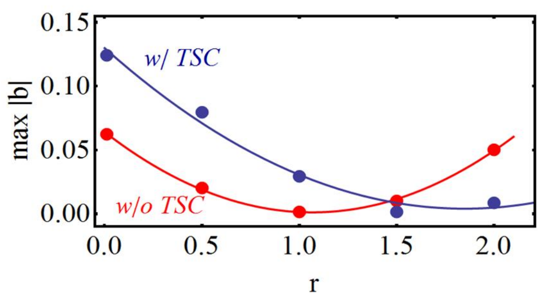

Figure 15: Amplitude of the observed microbunching as a function of |*R₅₆*| contributed by the compensation chicanes (blue data points). The parameter $r = |R_{56}/R^c_{56}|$ is the momentum compaction in units of the momentum compaction R^c_{56} corresponding to exact local *R₅₆* –compensation: the optimum setting is seen to occur at $r \simeq 1.5$. The red data points were obtained with an incomplete physics model excluding transverse space-charge (TSC) forces from tracking showing that in this case (longitudinal space-charge effects only) exact local *R₅₆* –compensation ($r = 1$) would be optimal.

5 References

[1] T. O. Raubenheimer, "Technical challenges of the LCLS-II CW X-ray FEL," in proceedings of IPAC2015, Richmond, VA, USA.

[2] P. Emma et al., in proceedings of FEL'14, THP025.

[3] M. Venturini, J. Qiang, C. Papadopoulos ,Y. Ding, P. Emma, Z. Huang, G. Marcus, A. Marinelli, Y. Nosochkov, T. Raubenheimer, L. Wang, M. Woodley, Proceedings of IPAC2015, p. 1843, Richmond, VA, USA (2015).

[4] M. Venturini, FEL15 Conference, Proceedings (2015).

[5] M. Venturini and J. Qiang, PRST-AB, 18, 054401, (2015).

[6] J. Qiang et al., PRST-AB 9, 044204 (2006).

[7] J. Qiang et al., J. of Comp. Phys., 163, 434 (2000).

[8] J. Qiang et al., PRST-AB 12, 100702 (2009)